Marine and Petroleum Geology 111 (2020) 529–543

Contents lists available at ScienceDirect

Marine and Petroleum Geology

journal homepage: www.elsevier.com/locate/marpetgeo

Research paper

Reservoir assessment of Middle Jurassic sandstone-dominated formations in the Egersund Basin and Ling Depression, eastern Central North Sea

Jørgen André Hansen[a,*], Nazmul Haque Mondol[a,b], Jens Jahren[a], Filippos Tsikalas[c,a]

[a] Department of Geosciences, University of Oslo, P.O. Box 1047, Blindern, NO-0316, Oslo, Norway
[b] Norwegian Geotechnical Institute (NGI), P.O. Box 3930, Ullevaal Stadion, NO-0806, Oslo, Norway
[c] Vår Energi AS, P.O. Box 101, Forus, NO-4064, Stavanger, Norway

ARTICLE INFO

Keywords:
Norwegian Central North Sea
Reservoir quality
Jurassic sandstone
Depositional trends
Compaction
Cementation
Fluid sensitivity
Seismic

ABSTRACT

Reservoir quality assessment was conducted from petrophysical analysis and rock physics diagnostics on 15 wells penetrating Middle Jurassic sandstone reservoir formations in different regions of the eastern Central North Sea. Seismic interpretation on available 3D and 2D seismic reflection data was utilized to map thickness variations and to draw broad correlations to structural features such as salt structures and faults. In the central Egersund Basin, the Sandnes Formation shows good reservoir properties (gross thickness = 107–147 m, N/G = 33–53%) while the Bryne Formation exhibits poorer reservoir quality (N/G < 20%). Both formations display variable reservoir properties and thicknesses on the northern flank of the Egersund Basin and in the Ling Depression (Sandnes Formation: gross thickness 16–26 m, N/G = 11–81%; Bryne Formation: 30–221 m, N/G = 25–70%). The time-equivalent Hugin and Sleipner formations are more locally developed in the southwest part of Ling Depression, and display good-to-excellent and intermediate reservoir quality, respectively. Furthermore, we use the outcomes of the conducted analyses to correlate observations to further exploration on various reservoir target formations and on seismic prediction of reservoir properties. Thus, the risk on reservoir presence and efficiency for the chased targets is considerably reduced. The main remaining risks within the study area are related to source rocks, their maturity, expulsion and migration of hydrocarbon, and the timing of trap formation.

1. Introduction

The North Sea, offshore Norway (Fig. 1a), is a mature oil and gas province which has been open for exploration since the mid 1960's. Still, the giant Johan Sverdrup field (Fig. 1b) was discovered as late as 2010. Existing fields are predominantly located on the flanks of the Jurassic-Cretaceous rift system, including the Viking, Central and Sogn grabens. These are sourced primarily by Late Jurassic source rock shales (Kimmeridge Clay Formation equivalents) which are mature in the deeper parts of the rift grabens. Large areas between the grabens and the platforms close to mainland Norway are, however, much more sparsely drilled (Fig. 1b). One of the main reasons for lower exploration activity is uncertainty associated with the maturity of the Jurassic source rock shales in this region, namely the time-equivalent Draupne and Tau Formations (Figs. 1c and 2).

The current study area encompasses basin regions around the Sele High, namely the Ling Depression, Egersund Basin, and parts of the Åsta Graben (Fig. 1). The target area is bounded by the Stavanger Platform to the east, Utsira High and Patch Bank Ridge to the north and northwest, and the Jæren and Sørvestlandet highs towards southwest (Fig. 1b). In the study area, the burial depth of the source rock is shallower than within the Viking Graben, and fluctuates around the depths and temperatures associated with the onset of hydrocarbon generation (Hansen et al., 2019). Certain important discoveries (mostly in the Egersund Basin) do however provide evidence of local source rock maturation and expulsion, although it has been described as limited in quantity (Ritter, 1988; Hermanrud et al., 1990). These discoveries include the Yme (9/2-1), Vette (17/12-1), Brisling (17/12-2), Mackerel (18/10-1) in the Egersund Basin, and Bark (17/3-1), Storskrymten (15/12-18S) and Grevling (15/12-21) in the Ling Depression (Fig. 1b). In the case of the SW Ling Depression, e.g., the Grevling discovery (quadrant 15), hydrocarbon migration from deeper Viking Graben regions is potentially more probable than a locally mature source rock due to the graben proximity.

Studies that specifically consider reservoir property variations are rare within and in the vicinity of the study area; however, Mannie et al.

* Corresponding author.
E-mail address: j.a.hansen@geo.uio.no (J.A. Hansen).

https://doi.org/10.1016/j.marpetgeo.2019.08.044
Received 10 April 2019; Received in revised form 22 August 2019; Accepted 23 August 2019
Available online 26 August 2019

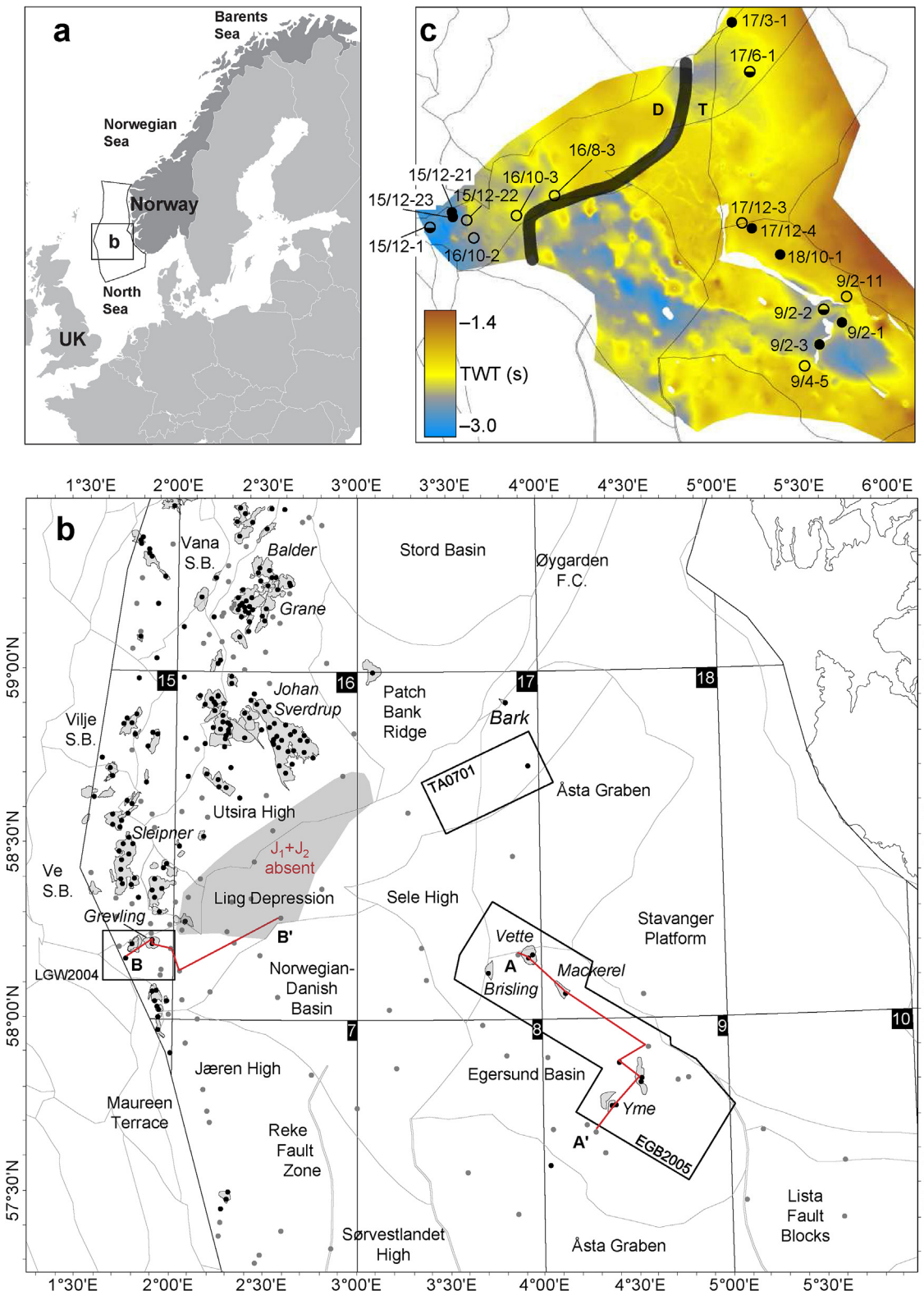

Fig. 1. (a) Location map of the greater study area situated within the Norwegian sector of the North Sea petroleum province (thin black outline). (b) Map outlining the Norwegian Central North Sea and South Viking Graben structural elements (NPD, 2019), with discoveries marked as light grey shading and exploration wells represented by points (grey = dry, black = discovery or hydrocarbon shows). 3D seismic surveys are outlined in black. Dark grey shading indicates absence of the Middle Jurassic reservoir formations within the study area. Red lines represent well correlation panels A–A′ and B–B′ (Fig. 5). (c) Wells selected for detailed investigation in this study, superimposed on the top Tau/Draupne Formation time surface indicating basin geometries. (For interpretation of the references to color in this figure legend, the reader is referred to the Web version of this article.)

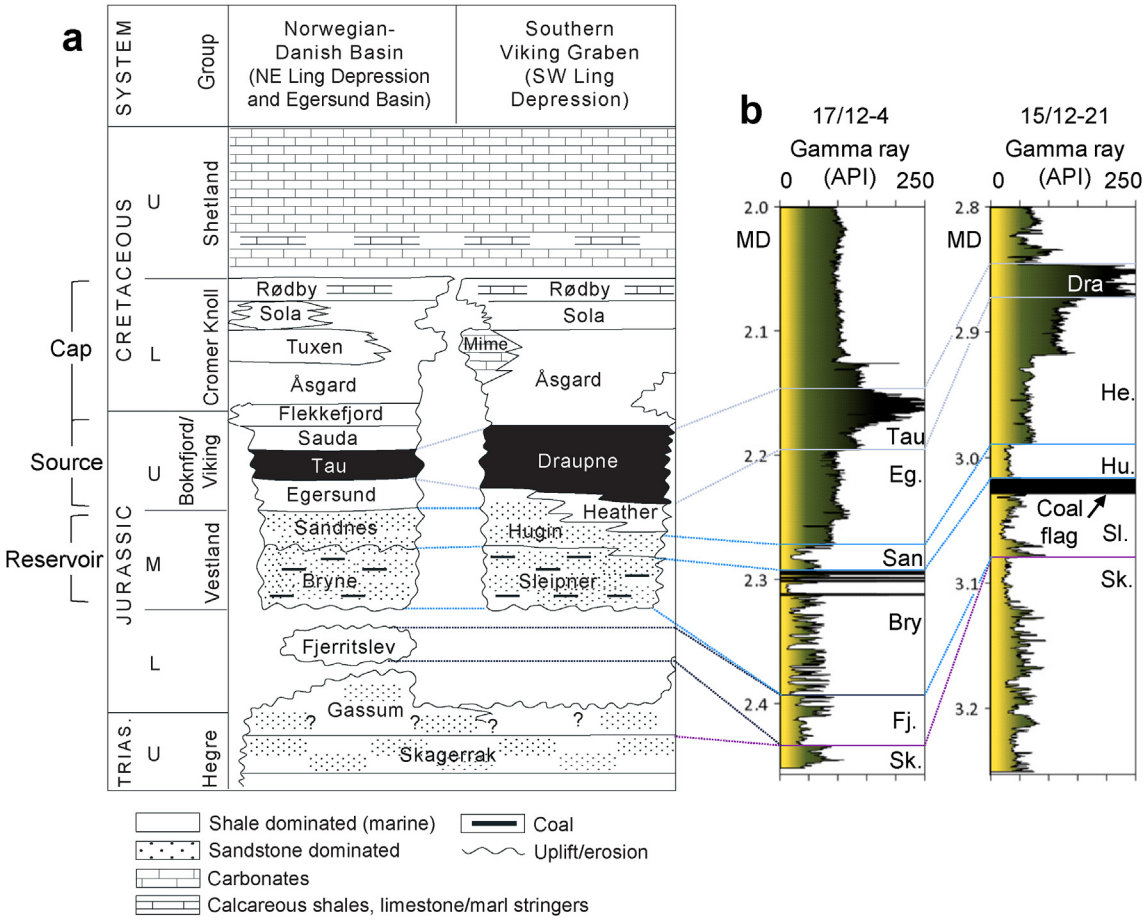

Fig. 2. (a) Upper Triassic–Upper Cretaceous lithostratigraphic chart (modified from Hansen et al., 2019), separated approximately along the black line in Fig. 1c. (b) Correlation of lithostratigraphy in two wells within the study area, 17/12-4 in the Egersund Basin, and 15/12-21 in the SW Ling Depression.

(2014) provide a facies analysis of commonly targeted Middle Jurassic reservoirs formations in the Egersund Basin. Additionally, detailed investigations of structural and halokinetic influences on deposition of relevant sedimentary units are demonstrated by Jackson et al. (2013) and Mannie et al. (2014, 2016). Furthermore, Kieft et al. (2010) studied the sedimentology and sequence stratigraphic development of the Hugin Formation in the South Viking Graben, adjacent to the northwestern border of the study area. Maast et al. (2011) on the other hand performed point-count analysis on 25 core samples from Hugin Formation sandstones in deeper parts of the South Viking Graben.

Reservoir quality is controlled by the burial (and thermal) history of the sediment, which drives porosity loss associated with different compaction mechanisms. The degree of mechanical compaction is a function of the sediment composition, grain size, and textural parameters, and relates closely to the depositional environment. Diagenetic processes, i.e., dissolution and precipitation of minerals (cementation), are chemical reactions driven by temperature and mineral stability (Bjørlykke et al., 1989; Peltonen et al., 2009). These occur over a wide range of depths and temperatures, and can have important implications on reservoir heterogeneity. Some diagenetic processes can also be porosity-preserving, e.g., formation of clay coats and dissolution of early precipitated carbonate cement (Morad et al., 2010).

A thorough reservoir characterization can be valuable to highlight any systematic variations in reservoir quality and extent in connection to areas where hydrocarbon generation and expulsion is suspected to have occurred. Even smaller discoveries in the North Sea can potentially be economically viable, when they are less remote and potentially closer to existing infrastructure. That is indeed the driver and motivation for the current study, with the conducted reservoir quality analysis of sand-prone Middle Jurassic units. We have applied an integrated approach of petrophysical analysis of well log data, rock physics diagnostics, and interpretation and attribute analysis of 3D seismic data to characterize potential reservoirs in the study area.

2. Geological setting and lithostratigraphy

The North Sea basin structure has been largely defined by two major rifting phases; the Late Paleozoic and the Late Jurassic-Early Cretaceous (Faleide et al., 2008). Additionally, the area has been subjected to exhumation in multiple phases; most recently in response to Oligocene and Miocene uplift of southern Norway and laterally variable Plio-Pleistocene glacial erosion (Jordt et al., 1995; Baig et al., 2019). The Norwegian-Danish Basin and second-order structural elements (e.g., Ling Depression and Egersund Basin; Fig. 1b) are mainly Late Paleozoic–Triassic features, less influenced by the characteristic North Sea Jurassic rifting, but have been affected by halokinesis (Fig. 3; Faleide et al., 2015).

The Jurassic sandstone-dominated formations in the Central North Sea area are part of the Vestland Group. In the southern and eastern part of the study area these are referred to as Bryne and Sandnes formations, which are broadly time-equivalent to the Sleipner and Hugin formations (Fig. 2). The latter two formations are present in the southwestern Ling Depression, and extend farther towards the north. For easier separation according to age, the older and younger formations are sometimes herein denoted $\mathbf{J_1}$ (Bryne and Sleipner formations) and $\mathbf{J_2}$ (Sandnes and Hugin formations), respectively. J_1 represents fluvial, deltaic and coastal plain deposits, whereas the J_2 interval can broadly be characterized as a result of shallow marine, nearshore

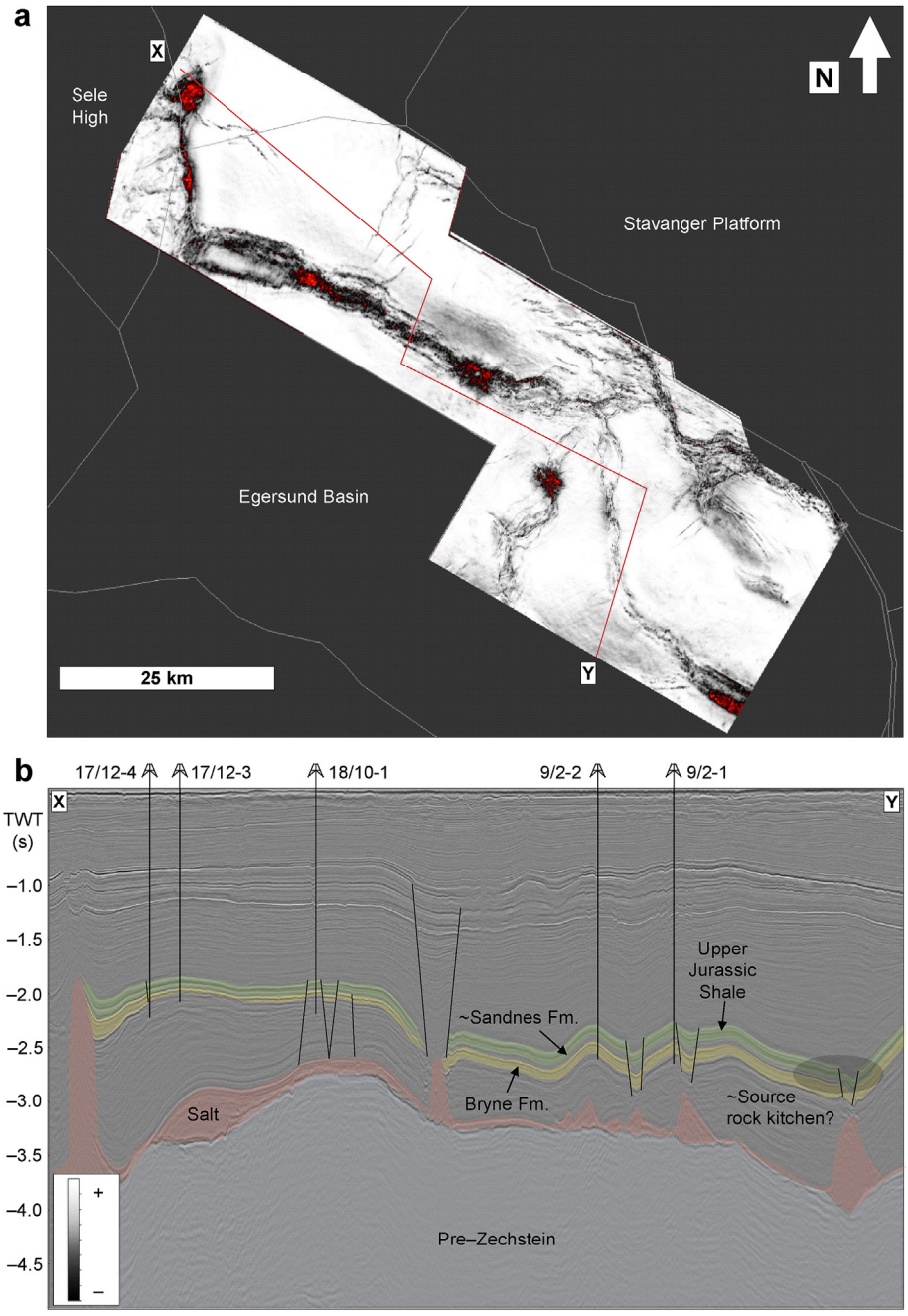

Fig. 3. Example from Egersund Basin seismic survey where the top Bryne Formation variance map (a) broadly indicates large scale structural elements (Sele High and Stavanger Platform), individual faults and fault zones, salt walls and salt diapirs. Cross section X–Y (b) illustrates general basin geometry and interaction between faults and salt structures; see Fig. 1c for lateral depth variation in the Jurassic section.

deposition (Vollset and Doré, 1984; Mannie et al., 2014).

Despite the similarities in depositional facies on time-equivalent formations, there are some differences in provenance. In particular, the Sandnes and Bryne formations are predominantly sourced from elevated areas towards the south and east, e.g., the Stavanger Platform and Norwegian mainland (Mannie et al., 2014), and the early Bryne Formation deposition started in the Egersund Basin prior to Bathonian-Oxfordian flooding of the North Sea Basin (Halland et al., 2011). On the contrary, the Hugin and Sleipner formations are more directly related to the transgression of the South Viking Graben and the accompanying southward retreat of the Brent Delta (e.g., Folkestad and Satur, 2008 and references therein). They are characterized by laterally different ages and controls on depositional patterns, and are potentially affected by Jurassic rifting to a greater degree than the Bryne and Sandnes formations (Folkestad and Satur, 2008; Kieft et al., 2010). Only the southernmost extent of these formations coincide with the study area, where the Hugin Formation consists mainly of deltaic wave-to tidal-influenced shoreline deposits that interfinger with continental facies of the underlying Sleipner Formation and the fine-grained marine deposits of the overlying Heather or Draupne formations (Kieft et al., 2010, Fig. 2).

Lower-Middle Jurassic and Triassic sediments are absent in certain regions of the Central North Sea due to erosion and/or non-deposition on structural highs, or due to uplift of the Mid-North Sea Dome during Early Jurassic (Ziegler, 1992; Mannie et al., 2014). This is evident for instance in the region around well 16/8-3 (Lupin) in the Ling Depression where none of the formations of interest are encountered (Fig. 1b). An elevated north-south trending structure between the Utsira High and

Table 1
Overview of well database selected for the study. Note availability of shear wave velocity (V_S). Prospect names (for discoveries and dry wells alike) are noted to ease further references to individual wells.

Well	Prospect	Area	Content	TD (m)	TVD (m)	Exhumation (m)	Seismic survey	Year drilled	V_S
9/4-5	–	EGB	Dry	5881	5874	250	2D	2006	–
9/2-3	Yme	EGB	Oil	3424	3421	300	EGB2005	1990	–
9/2-2	–	EGB	Oil shows	3577	3548	500	EGB2005	1987	–
9/2-1	Yme	EGB	Oil	3756	3755	500	EGB2005	1987	–
9/2-11	Aubrey	EGB	Dry	2861	2836	620	EGB2005	2010	✓
18/10-1	Mackerel	EGB	Oil	2800	–	450	EGB2005	1980	–
17/12-3	Vette (Bream)	EGB	Dry	2730	–	375	EGB2005	1980	–
17/12-4	Vette (Bream)	EGB	Oil	2470	2470	400	EGB2005	2009	✓
17/6-1	Svaneøgle	NE Ling D.	Oil shows	3065	3064	550	TA0701	2011	✓
17/3-1	Bark	NE Ling D.	Gas	2852	2852	500	2D	1995	–
16/10-2	–	SW Ling D.	Dry	3150	3148	–	2D	1991	–
15/12-21	Grevling	SW Ling D.	Oil	3310	3310	–	LGW2004	2009	✓
15/12-22	Storkollen	SW Ling D.	Dry	3035	3035	–	LGW2004	2010	✓
15/12-23	Grevling	SW Ling D.	Oil	3485	3478	–	LGW2004	2010	✓
15/12-1	–	SW Ling D.	Oil shows	3269	3269	–	2D	1975	–

EGB = Egersund Basin; NE Ling D. = Northeast Ling Depression; SW Ling D. = Southwest Ling Depression.

the Jæren High was prominent in this region during Bathonian and Callovian times (Folkestad and Satur, 2008).

3. Database and methods

The utilized database consists of 15 vertical or near-vertical exploration wells distributed across the study area, as well as many 2D seismic lines and three 3D seismic cubes (Fig. 1b; Table 1). Additionally, core plug measurements of porosity and permeability were compiled from public reports obtained via Diskos (NPD, Norwegian Petroleum Directorate). The database was selected to cover a wide range of reservoir depths, and to cover regions of interest for hydrocarbon exploration either where there are possibilities for external migration or signs of locally mature source rock (Hansen et al., 2019). Firstly, the reservoir formations were classified in terms of lithology, porosity and fluid content from petrophysical well log data, using consistent net-to-gross definitions based on suitable cutoff-values.

Due to different depositional environments and the fact that potential flow barriers such as thin shales and coal layers are commonly observed between the J_1 and J_2 formations (Fig. 2), these are treated as separate reservoir sections in the conducted petrophysical analysis. The Hugin and Sleipner formations are additionally more locally developed and do not always coincide (missing from wells 15/12-23 and 15/12-22, respectively). We also present cumulative or total reservoir thicknesses and properties, i.e., the combination of J_1 and J_2. To predict maximum sandstone burial depth, exhumation magnitude was estimated based on velocity–depth data compared to experimental (normal) compaction trends and published estimates (e.g., Doré and Jensen, 1996; Mondol et al., 2008; Kalani et al., 2015a; Hansen et al., 2017; Baig et al., 2019).

Shale volume (V_{sh}) was calculated using the gamma-ray log and corrected after Larionov (1969) for older rocks, and supplemented with interpretations of properly scaled neutron-density overlays where applicable. Porosity (Φ) was estimated from the average of neutron porosity (Φ_N) and porosity from density (Φ_D), calculated as

$$\Phi = \sqrt{[(\Phi_D^2 + \Phi_N^2)/2]}, \quad (1)$$

and subsequently quality controlled by comparing with core plug porosity where available (Fig. 4). Coal layers, particularly common in the Bryne and Sleipner formations, were excluded based on distinctive density, neutron and sonic signatures. Similarly, carbonate cemented sandstone layers and carbonate stringers display oppositely abnormal values in the same logs (Maast et al., 2011). We employed cutoffs for shale volume and porosity for defining net reservoir (where gross equals total formation thickness), and utilized water saturation (S_w) to define net pay where applicable. Core plug measurements suggest that 11–12% porosity is required to expect permeability around 1 mD (Fig. 4a).

Water saturation (S_w) was calculated from Archie's relation as

$$S_w = [(a \times R_w)/(R_d \times \Phi^m)]^{1/n}. \quad (2)$$

Here, R_d is deep resistivity, and Φ is effective porosity. The constant a represents the tortuosity factor, while m and n denote the cementation factor and saturation exponent, respectively. Commonly utilized values suitable for consolidated sandstone were used as coefficients, $a = 0.81$ and $m = n = 2$ (Asquith and Krygowski, 2004), which provided a satisfactory level of accuracy. Formation water resistivity (R_w) was determined from core reports (NPD, 2019), from brine filled clean sandstones in the same well and stratigraphic level where possible, or approximated as 0.04 Ω-m where no reference was available.

The selected cutoff values applied for net-to-gross estimation were $V_{sh} < 0.3$, $\Phi > 0.12$ and $S_w < 0.6$. Additionally, a minimum reservoir and pay zone thickness of 0.5 m was applied to discriminate the thinnest sands while still allowing for heterogeneous reservoir intervals.

Seismic mapping of target horizons and coherency attributes were employed to understand lateral variations in depth, thickness, and large-scale structural influences. Three poststack 3D seismic surveys (TA0701, EGB2005 and LGW2004) available in the public domain (courtesy of NPD via Diskos) were used for seismic interpretation of reservoir formations (J_1 and J_2) and adjacent key horizons. In total, the surveys cover approximately 3600 km^2, including a large part of the Egersund Basin, the northeast part of the Ling Depression, and the southeast segment of the Ling Depression. Publicly available 2D lines (North Sea Renaissance survey) were used for understanding regional variations outside of the 3D seismic data cubes. Dip illumination and variance attribute maps (Fig. 3a) were used to broadly delineate the main structural elements, faults and salt structures (Fig. 1b). The top Bryne horizon is picked with high confidence on wide-spread coal layers in the upper part of the formation. The Sandnes Formation can be mapped individually in the central part of the Egersund Basin due to greater thickness, but this is not the case in the NE Ling Depression survey (TA0701). In the SW Ling Depression seismic (LGW2004), the resolution and reflector continuity below the Upper Jurassic shale is relatively poor, and consequently the Hugin and Sleipner formations are more difficult to pick with confidence. Due to its rapidly varying thickness (resolution limits visibility) and lack of confidence in horizon tracking, drawing any conclusions from the Hugin isochore was inadvisable.

Based on petrophysical analysis, where we obtained important reservoir parameters related to depositional diversity and degree of compaction, we take advantage of rock physics to link geological

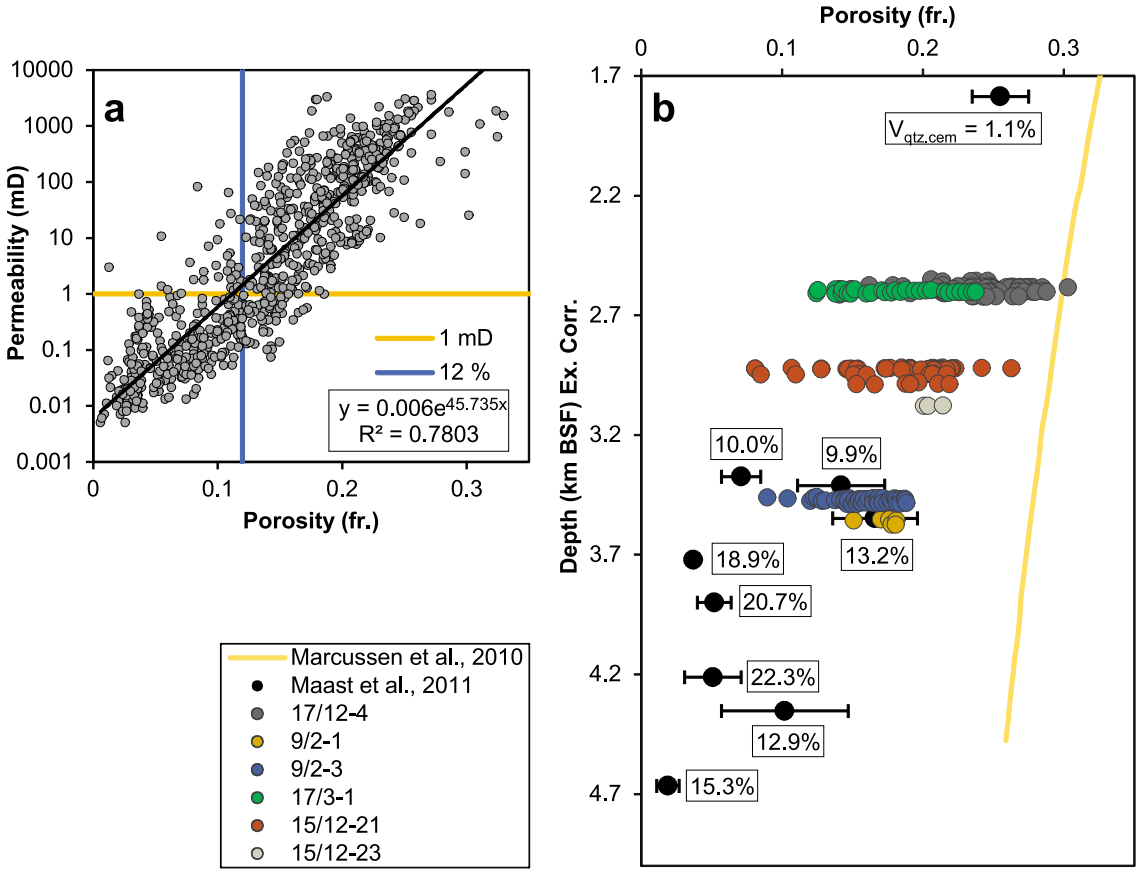

Fig. 4. (a) Core porosity versus permeability showing all available measurements, i.e., not filtered for coal or clay content. (b) Core plug porosity versus depth for clean Middle Jurassic sandstones compared to an experimental compaction curve representing mechanical compaction of loose Etive sandstone (Marcussen et al., 2010). Porosity ranges from thin section point-count analysis of Hugin Formation arenite sandstones (non-carbonate-cemented) are shown as black points and marked with values representing average quartz cement volume (Maast et al., 2011).

variations with elastic parameters that relate to seismic reflection data. Theoretical rock physics models or templates (Ødegaard and Avseth, 2004) can be used to compare different wells, such as in V_P/V_S versus acoustic impedance (AI) crossplots that enable simultaneous interpretation of lithology, porosity (cementation) and fluid sensitivity (i.e., separating brine- and hydrocarbon-saturated sandstones). Furthermore, AVO half-space modeling using the Shuey approximation (Shuey, 1985) was used in selected wells to evaluate the sensitivity of AVO signatures to fluid content in the case of oil versus brine (for angle-stacks up to 30°).

4. Results

In the following, we present the integrated results from the conducted well log characterization, seismic interpretation and rock physics diagnostics of Middle Jurassic reservoir sandstones.

4.1. Petrophysical reservoir quality evaluation

Fig. 5 displays correlations of the Middle Jurassic sandstone–dominated formations in key wells from the Egersund Basin and southwest Ling Depression. Coal layers are marked with dark grey shading. An increasing total gross thickness is evident in wells located towards the center of the Egersund Basin (9/2 block, Yme area). J_2 is thinner than J_1 in all but two wells (15/12-22 and 9/4-5). Wells 9/2-11 (Aubrey) and 9/2-3 do not penetrate the base Bryne horizon, but the Bryne Formation is still inferred from seismic to be thicker than the Sandnes Formation. The latter gradually increases in thickness from the NE Ling Depression (not shown in Fig. 5) and the Vette/Bream area (17/12-3 and 17/12-4), towards a maximum of 147 m in well 9/2-1 (Yme; Fig. 5). Well 9/2-3 is not included in Fig. 5, but has almost identical thickness and log signatures as well 9/2-1 in the Sandnes Formation.

The Hugin Formation on the other hand displays large local thickness variations, from 154 m in the Storkollen well (15/12-22) to being absent in well 15/12-23 (on the Grevling discovery) 6.3 km farther west (Fig. 5). It is also drastically thinner or absent towards the north-east in the Ling Depression (wells 16/10-3 and 16/8-3S included for context in Fig. 5). The J_1 interval is consistently thinner in the Ling Depression than in the Egersund Basin, with the exception of the southernmost studied well 9/4-5 (53 m). The Sleipner Formation is only present in the three westernmost wells (Fig. 5).

Output values from the petrophysical analysis are presented as averages in Table 2. The corresponding Fig. 6 visualizes relationships between various reservoir parameters to better compare and contrast different formations. Highlighted clusters and trends indicate differences in reservoir potential corresponding to basin location for the Bryne and Sandnes formations.

The total Middle Jurassic net reservoir thickness is generally greater in the Egersund Basin (60–116 m) compared to the Ling Depression (12–52 m). A notable exception is found in well 15/12-22 (Storkollen), with 153 m of high-porosity Hugin Formation sandstone. The net-to-gross (N/G) reservoir parameter serves as a more general indicator of reservoir quality irrespective of formation thickness. J_2 displays a wide range of N/G values from 11 to 99% with an average of 60% across all wells (Table 2; Fig. 6a). The reservoir maximum burial depth does not correlate with N/G value (Fig. 6c). On the other hand, J_1 varies from 7 to 70% N/G, with an average value of 36% (Fig. 6b). In this case, we

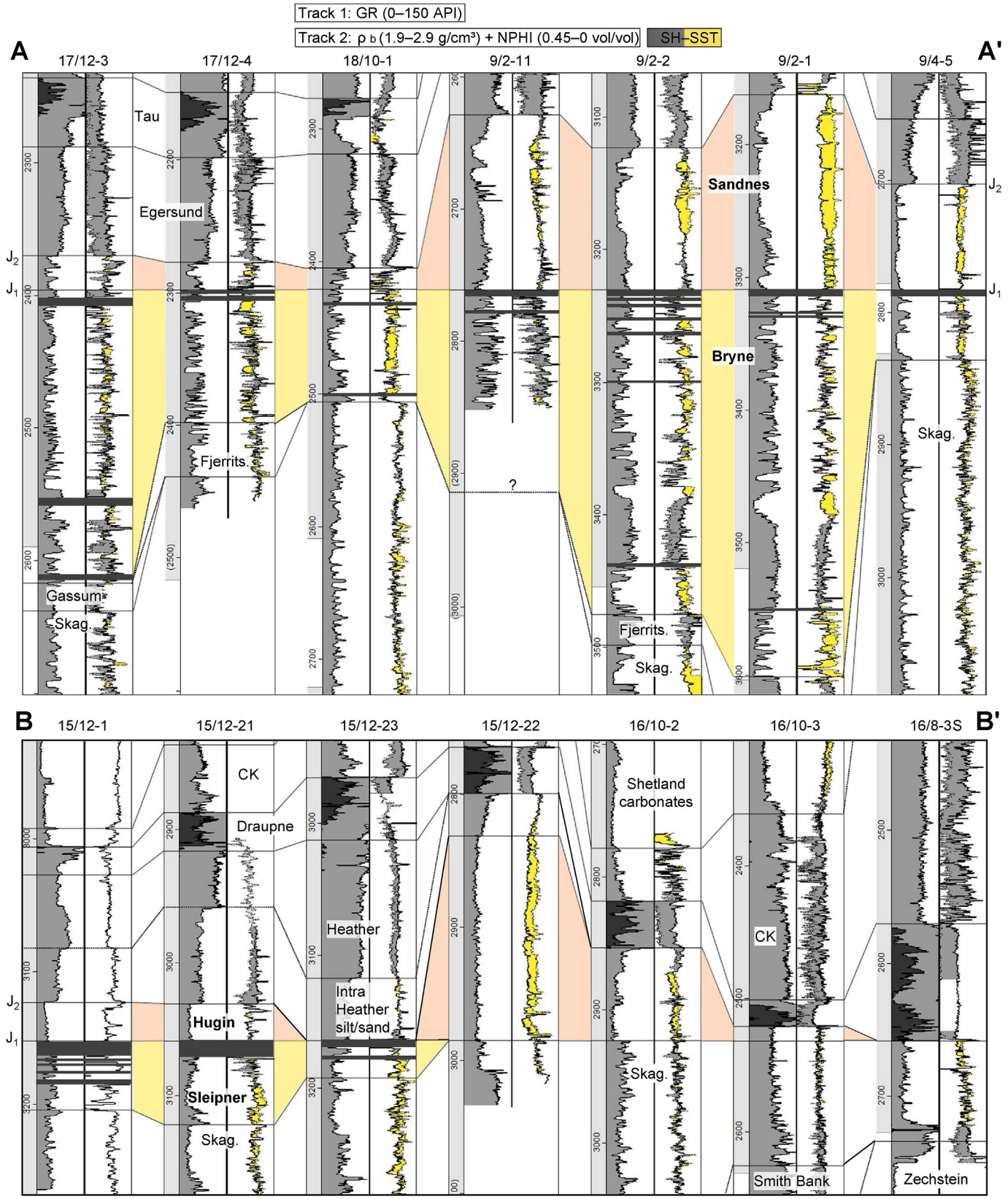

Fig. 5. Well correlation panels for Middle Jurassic reservoir formations, flattened on the J_1–J_2 transition. A–A′ is located in the Egersund Basin, and is oriented from the northwest flank through the central part to the south flank. B–B′ is oriented west–east in the SW Ling Depression. Well correlation panel locations are shown in Fig. 1b. J_1 (Bryne and Sleipner formations) and J_2 (Sandnes and Hugin formations) are indicated by yellow and light red shading, respectively. (For interpretation of the references to color in this figure legend, the reader is referred to the Web version of this article.)

Table 2
Results of the petrophysical analysis, with values reported as averages per zone. Depths are stated in meters below sea floor, corrected for estimated exhumation.

Location	Well (prospect)	Top depth (m)	Ex.corr.	Gross (m)			Net reservoir (m)			N/G reservoir[c] (%)			V_{sh} reservoir zone (%)			Φ reservoir zone (%)			Net pay (m) = S_w < 0.6		
				J_1[a]	J_2[b]	Tot.	J_1	J_2	Tot.	J_1	J_2	Tot.	J_1	J_2	Tot.	J_1	J_2	Tot.	J_1	J_2	Tot.
EGB S. Flank	9/4-5	2832		53	80	133	35	75	110	66	93	83	10	6	8	21	22	21			
Egersund Basin Central	9/2-3	3448		[d]33	121	154	4	64	68	13	53	44	10	9	9	17	15	15		5	5
	9/2-2	3551		245	107	352	36	35	71	15	33	20	8	16	12	16	16	16			
	9/2-1 (Yme)	3534		292	147	439	21	67	88	7	46	20	6	12	10	13	13	13	2	44	46
	9/2-11 (Aubrey)	3122		[d]90	132	222	18	63	80	20	48	36	14	16	16	17	18	18			
EGB N. Flank	18/10-1 (Mackerel)	2734		85	16	101	59	2	61	70	11	61	10	14	10	22	22	22	9	1	10
	17/12-3	2608		221	26	247	102	15	116	46	57	47	11	13	11	22	20	22			
	17/12-4 (Vette)	2549		100	21	121	50	10	60	50	49	50	10	15	11	23	20	23	20	1	21
NE Ling Depression	17/6-1 (Svaneøgle)	2890		79	17	96	20	3	23	25	19	24	5	20	7	19	14	18			
	17/3-1 (Bark)	2589		30	23	53	16	18	35	54	81	66	11	8	10	21	23	22	1		1
SW Ling Depression	16/10-2	2749			70	70		52	52		75	75		10	10		23	23			
	15/12-21 (Grevling)	2902		63	28	91	20	24	44	31	88	49	14	14	14	16	21	19	20	24	44
	15/12-22 (Storkollen)	2723			154	154		153	153		99	99		11	11		24	24			
	15/12-23	3051		28		28	12		12	43		43	10		10	17		17	8		8
	15/12-1	3003		52	29	81	24	14	38	27	82	47	15	6	9	19	20	20			
Average				113	69	156	32	43	70	36	60	51	10	12	10	19	19	19			

[a] Bryne/Sleipner.
[b] Sandnes/Hugin.
[c] V_{sh} < 0.3, Φ > 0.12.
[d] Base Bryne not penetrated.

observe a clear decrease in the N/G parameter from Bryne reservoirs between ~2.6 km and 3.7 km (Fig. 6d). The Sleipner Formation reservoirs at intermediate depths fall along the same trend.

After filtering out shaly and low-porosity intervals, the net reservoir porosity is observed to vary fairly consistently with the reservoir maximum burial depth, between 13 and 24% (Fig. 6e). Where both J_1 and J_2 successions have representative net reservoir thicknesses, only minor variations are observed in average porosity. As seen in Table 2, there is a maximum difference of 5% between the older and younger reservoir sandstones in any given well location.

4.2. Thickness variations

Fig. 7 displays time-thickness (isochore) maps of different reservoir intervals. 2D seismic lines are used to cover the southwest part of the Egersund Basin, the Åsta Graben between the EGB2005 and TA0701 3D surveys, and part of the NE Ling Depression. Drawbacks include poorer lateral resolution and some inconsistencies when compared to the 3D surveys, but the 2D seismic reflection dataset provides better semi-regional context for the extent of the Bryne Formation. Fairly uniform Bryne Formation thickness can be observed in the Åsta Graben and the NE Ling Depression. We take note of likely structural influences, e.g., increased thickness east of a NW-SE trending fault located east of well 17/6-1, as well as towards the Øygarden Fault Complex in the north (Fig. 7a). In the Egersund Basin, the Bryne Formation varies quite substantially, displaying greater thickness overall in the southern part, and particularly along salt walls (c.f. Fig. 3a). Where mapped, the Sandnes Formation exhibits very similar behavior (Fig. 7b).

The Sleipner time–thickness (isochore) map (Fig. 7c) reflects the overall thinning out towards the eastern part, as observed in well correlation (Fig. 5). Additionally, we can identify similar local thickening towards larger faults. Salt related structures were observed, as was the case in the Egersund Basin, which causes problems with reflector discontinuities and consequent interpretation above salt (gaps in thickness maps). Some of the marked faults correlate with deeper salt structures, whereas other could stem from Jurassic extension and creation of the adjacent Viking Graben. Thickness variations in the areas that are not heavily influenced by faulting could indicate depositional features. For instance, channel-like geometries are sporadically identified within the Sleipner Formation in the seismic (Fig. 7c).

4.3. Rock physics relationships and sensitivity

Typically for poststack seismic, the output data that can be analyzed consist of acoustic impedance volumes derived from seismic inversion. Well-log derived acoustic impedance from primary cap rock and reservoir formations (without filters) at different depths is shown in Fig. 8a, revealing rough depth trends for sand and shale that are shifted slightly in relation to each other. No coherency is however observed in AI (acoustic impedance) as a function of smaller shale volume variations within reservoir formations, either when examining individual wells or as exemplified compositely for all wells in Fig. 8b. AI varies predominantly between 7 and 11 g/cm^3 × km/s for reservoir sections encountered above 3.2 km maximum burial, and from approximately 9–13 g/cm^3 × km/s in formations with greater burial (Fig. 8b). Particularly when considering the cleaner sand proportion (V_{sh} < 0.3), AI instead correlates highly with porosity (Fig. 8c). A decrease in porosity from 30% to 5% yields an increase in AI of approximately 5 g/cm^3 × km/s.

When shear velocity information is incorporated, using V_P/V_S–AI crossplots, we can get combined information about shale content, porosity, and fluids, and we are able to compare to theoretical compaction trends for clean quartz sand (Ødegaard and Avseth, 2004). Fig. 9 indicates differences in elastic properties as a function of clay content, porosity and associated cementation, as well as fluid content. An empirical shale trend based on organic-lean shale data (Hansen

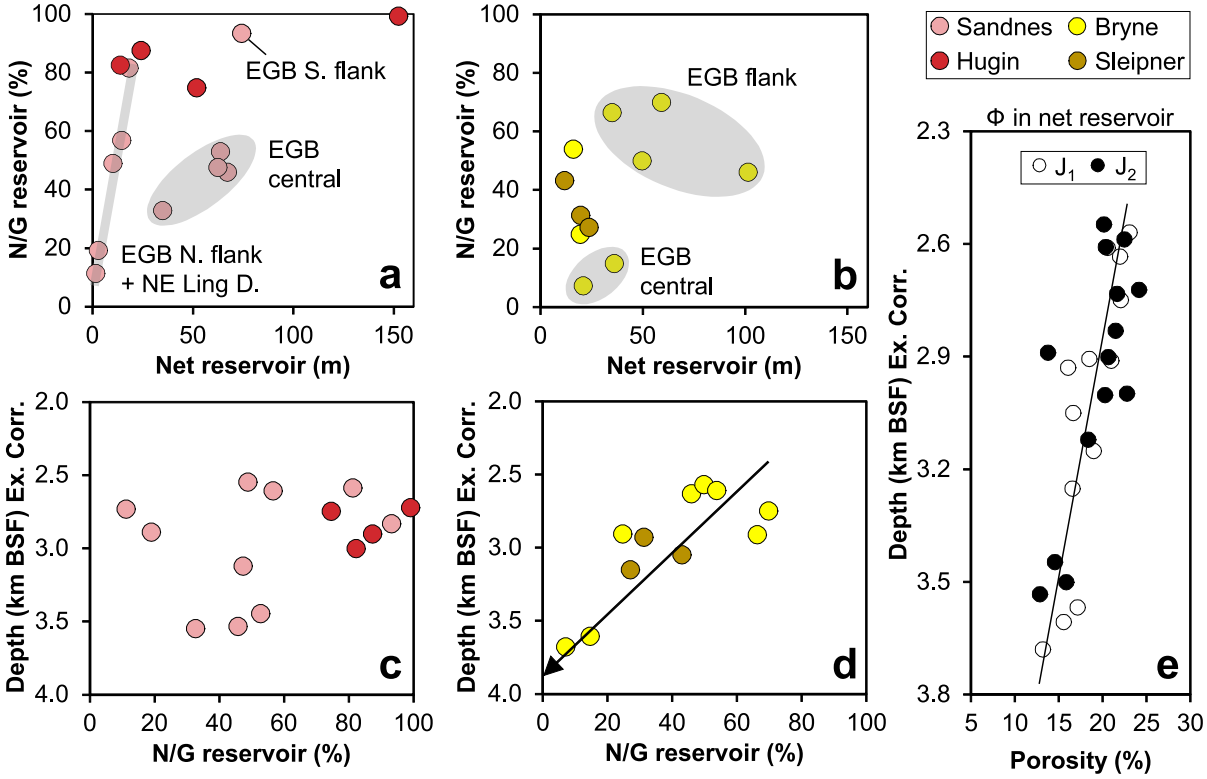

Fig. 6. Relationships between reservoir parameters separated according to formation and age; net reservoir thickness versus net–to–gross (N/G) reservoir (a, b), net–to–gross compared to top reservoir depth (c, d), and average net reservoir porosity as a function of maximum burial depth (e; BSF = below seafloor, Ex. Corr. = corrected for estimated exhumation). Wells that do not penetrate the base Bryne horizon have been excluded from plots (b) and (d).

et al., 2019) and a generalized brine–oil sandstone template assuming 30 MPa effective pressure are superimposed for reference. We observe improved discrimination of shaly intervals in reservoir formations, which plot towards slightly higher V_P/V_S values than clean sands (Fig. 9a). Porosity deterioration as a function of burial and cementation relates to AI as shown in Fig. 8. Additionally, we observe a corresponding decrease in V_P/V_S from around 2.1 to 1.65 for sandstone porosities between 30% and 5%, albeit with substantial scatter in the y–axis direction (Fig. 9b).

In well 17/12-4, we observe that data from brine-saturated sandstones plot predominantly above the brine sandstone model (Fig. 9c). Oil sandstone data fall mainly between the 100% brine and 100% oil line, although some overlap scatter is evident. The brine and oil clusters are consequently separated by approximately 1.6 g/cm^3 × km/s in AI and 0.1 in V_P/V_S when considering averages. In Fig. 9d, we take note of two features; firstly, the separation between two brine-sandstone populations in the Storkollen well as a result of porosity is clearly pronounced (ΔAI = 1.1, $\Delta V_P/V_S = -0.13$). The lower-porosity population has an average Φ = 23%. Secondly, the overlap between the lower part of the brine-sand cluster and the oil-sand data is substantial, both of which plot primarily above the brine sandstone model (Fig. 9d). Only a handful of data points from the oil leg plot closer to the oil-sand model.

4.4. Synthetic AVO modeling

The intercept (R_0) versus gradient (G) crossplot in Fig. 10 displays the forward-modeled AVO signatures of top reservoir interfaces, in-situ and fluid substituted, corresponding to the wells in Fig. 9c and d. A simplified background shale trend assuming $V_P/V_S = 2$ is superimposed. The Bryne Formation contains both oil- and brine-saturated sandstones in-situ, where the oil saturation in the former was interpreted to be high from petrophysical data. For comparison, these two chosen oil- and brine intervals have been substituted to 100% brine and 90% oil, respectively (Fig. 10a). The properties of a shaly layer between the Sandnes (brine in-situ) and Bryne Formation (oil in-situ) were used for the cap rock in the modeling. The fluid effect from substitution is predicted to be smaller (circle–circle and triangle–triangle) than what is apparent when comparing the in-situ brine and oil sandstones (Fig. 10a; triangle–circle). In both cases, AVO class II is predicted for brine sandstone, whereas class III is predicted for oil. The Sandnes Formation, which is brine-filled in-situ, is predicted to move from AVO class I to IIp in the case of oil (Fig. 10a; squares). In this case the cap rock was assigned properties corresponding to the lowermost Egersund Formation shale.

For all cases in Fig. 10b, representing the Storkollen and Grevling prospects, the predicted fluid separation is fairly small. Properties of Heather Formation shale were used to represent the cap rock in both wells. We can see that AVO class III is predicted in the Grevling well, whereas higher-porosity Hugin Formation sandstones in the Storkollen well plot as class IV.

5. Discussion

Firstly, we review the implications of the conducted reservoir analysis for hydrocarbon exploration and how different formations compare and vary. Secondly, the feasibility of using seismic properties to predict reservoir parameters on seismic reflection data is discussed based on observed rock physics trends. Finally, we put the reservoir analysis into context with plausible areas of hydrocarbon generation and discuss potential challenges.

5.1. Reservoir quality assessment

Based on the range of burial depths of Middle Jurassic Formations (> 2.5 km), the expectation is that all encountered sandstones are at least somewhat cemented. The observed porosity range (Table 2) and

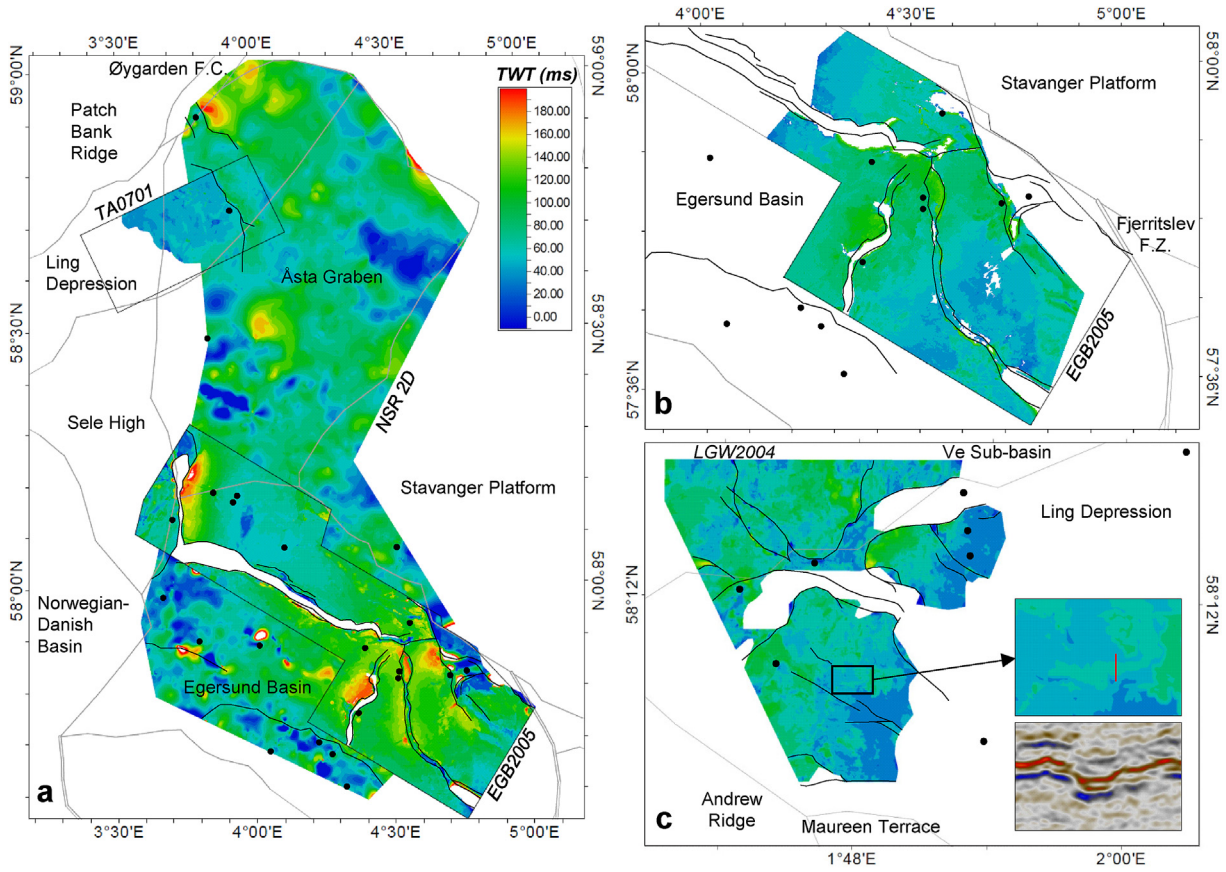

Fig. 7. Time-thickness (isochore) maps representing (a) the Bryne Formation in the Egersund Basin and NE Ling Depression based on two 3D surveys and the available 2D seismic dataset, (b) the Sandnes Formation based on the EGB2005 3D survey, and (c) the Sleipner Formation in the SW Ling Depression based on the LGW2004 3D survey (see Fig. 1b for relation to structural elements). Note possible resolution of channel-like geometries, appearing as very subtle features in the thickness map.

deviations in core plug porosity compared to a suitable mechanical compaction trend (Fig. 4b) also indicate that chemical compaction and quartz cement is influential at all relevant reservoir depths in the study area. Petrographic information from Middle Jurassic sandstones within the study area and nearby vicinity is unfortunately scarce. Only limited information restricted to the Hugin Formation is available from nearby wells (Maast et al., 2011). The latter information contributes to an understanding of the spread in core plug porosity seen in Fig. 4b. The Hugin Formation data show high inter-granular volume (IGV) post mechanical compaction (ranging between 28% and 38% with an average close to 33%) and also rather high detrital clay content (range of 1–11% with an average of 7%). The content of cements other than quartz is low, less than 2%. Therefore, the variability seen in the core plug porosity data in Fig. 4b must be related to variations in IGV and detrital clay content. A variable detrital clay effect on the rate of quartz cementation, which is probably related to the distribution between pore-filling and pore-lining clay may also contribute to the observed porosity variability and associated permeability ranges.

The Sandnes Formation has clearly the most favorable and consistent reservoir potential where it is well-developed in terms of thickness, i.e., mainly around the central Egersund Basin. On the flanks of the basin, as well as in the NE Ling Depression, more variable N/G is observed, and an additional limiting factor is the drastic decrease in thickness (Fig. 6a). The reason for lower N/G is likely related to the depositional environment and varying amounts of sand (e.g., Svaneøgle well 17/6-1), as it shows little correlation with formation depth (Fig. 6c). These observations fit well with core descriptions and facies associations (Mannie et al., 2014), where shoreface facies is found to dominate the Sandnes Formation except for certain wells on the north flank of the Egersund Basin where offshore facies are prevalent. In well 9/4-5 on the south flank of the Egersund Basin, the Sandnes Formation properties and thickness are better developed and/or preserved than on the north side.

Conversely, the Bryne Formation has poorer reservoir quality in the central Egersund Basin, predominantly as a result of deeper burial and consequent porosity deterioration (Fig. 6b and d). Most likely, the porosity relates to pore-filling quartz cement (Fig. 4b). On the flanks of the basin however, the Bryne Formation shows intermediate to high cumulative reservoir sandstone thickness, and increased N/G and sandstone porosity. Heterogeneity and possible fluid barriers (fine-grained coastal deposits) could be an issue; however, well 17/12-4 encounters multiple levels of oil-bearing sandstones interbedded with shale.

Thickness variations of Sandnes and Bryne formations in the Egersund Basin are largely coherent with the location of salt structures. As discussed in Mannie et al. (2014), the movement of salt created accommodation space, explaining the increased thicknesses observed on the flank or to the sides of salt structures. The Norwegian-Danish Basin similarly has a high density of salt structures which, depending on the extent of reservoir formations, could have had the same positive impact on the development of sand-dominated formations. The influence of salt in the Ling Depression is less prominent, particularly in the northeast which is consistent with the more uniform thickness of the Bryne Formation observed in the northeast Ling Depression (Fig. 7a).

Considering areas farther southwest in the Ling Depression, the Hugin Formation displays consistently good reservoir quality within the examined wells, with excellent properties and thickness in the Storkollen well 15/12-22 (Table 2; Fig. 6a). Rapid thickness variations

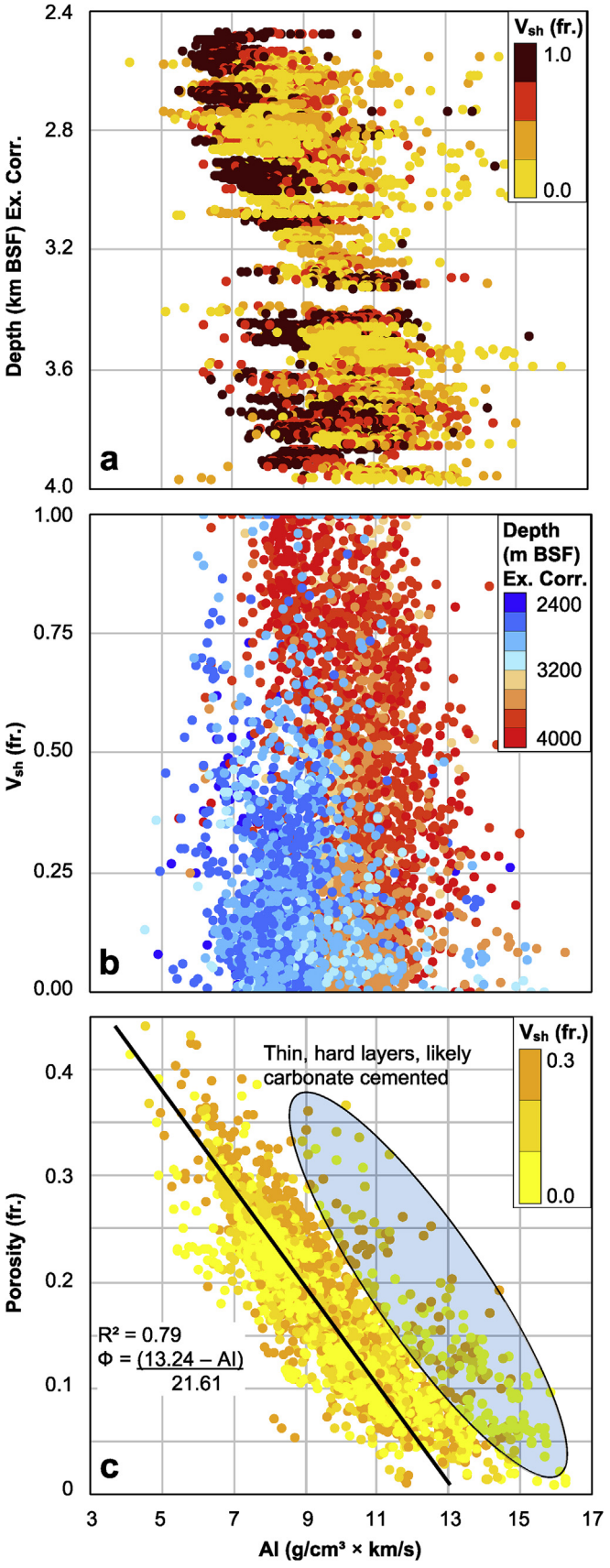

Fig. 8. (a) Crossplot of AI versus depth providing an overview of the Middle Jurassic reservoir formations and immediate cap rocks (Egersund and Heather formations) in all 15 wells, color coded with V_{sh}. (b) AI versus V_{sh}, reservoir formations only, color coded with depth. (c) AI versus porosity for clean sand data only, displaying a best fit $R^2 = 0.79$. (For interpretation of the references to color in this figure legend, the reader is referred to the Web version of this article.)

based on wells and poorly constrained seismic expression result in uncertain lateral extent of this formation. The Sleipner Formation, while easier to constrain on seismic, is similarly not regionally continuous. Our limited sample pool indicates no better than intermediate, albeit consistent, reservoir quality compared to the time-equivalent Bryne Formation (Fig. 6d). If the channel structures observed in the seismic data (Fig. 7c) correspond to fluvial deposits, these would be of substantial thickness when considering the seismic resolution. Consequently, the indication is a depositional environment that could accommodate larger, concentrated channels.

5.2. Predicting reservoir properties from seismic reflection data

Initially, we assessed the complete dataset, looking for trends both in Middle Jurassic reservoir formations and immediate relevant cap rock formations. As the stratigraphy in the region is well understood and some well control exists in most areas, seismic mapping provides the main framework for separating sand- and shale-dominated units. Subsequently, more focus was given to relating elastic properties to porosity variations and fluid anomalies. Overall, we find that seismic properties display fair separation between different lithologies, as well as good sensitivity to porosity. When discussing cementation in the context of reservoir quality in the study area, the primary concern is the precipitation of quartz cement driven by the transformation of thermally unstable smectite to illite, starting at around 70 °C (Bjørlykke, 1998), which is the main process for porosity-reduction when considering burial depths greater than ~2–2.5 km (Bjørlykke et al., 1989; Marcussen et al., 2010). Grain-coating clay or microquartz can prevent or retard cementation, thereby serving as porosity-preserving mechanisms (Morad et al., 2010; Maast et al., 2011). We do not explicitly consider carbonate cement, which relates to processes that occur at much shallower depths, and unless dissolved during burial, is often found to severely compromise the primary porosity of the sand (e.g., Bjørlykke et al., 1989). Additionally, the carbonate stringers and carbonate cemented sandstone layers identified in the studied wells (see "Database and methods") are very thin compared to the gross sand thickness (Fig. 5). Bulk density and AI in these layers typically surpass 2.5–2.6 g/cm^3 and 12–14 g/cm^3 × km/s, respectively.

AI alone is found to be a poor attribute for distinguishing detailed intra-reservoir shale variations, regardless of examination depth (Fig. 8b). Conversely, it serves as a very good predictor of porosity in clean sandstone (Figs. 8c and 9b). In certain areas and/or formations inferred to be less prone to heterogeneity and clay contamination, AI can be used more confidently to predict and map porosity variations. Depending on the resolution of seismic data and interpretations, candidates for this approach would be the Hugin Formation, the Sandnes Formation in the central Egersund Basin, and possibly the Bryne Formation on the Egersund Basin flanks. When doing a combined evaluation of shale content, depth and porosity in the V_P/V_S–AI domain, superimposed on theoretical models for ease of reference, we attain slightly better discrimination of shaly intervals, as well as an accurate porosity resolution. Thus, geophysical data could be suitable for simultaneously discriminating good sands and accurately predicting porosity variations when evaluating prospects, particularly in locations not too far from existing wells. This approach assumes the existence and availability of prestack seismic data.

Ultimately, the main goal of seismic reservoir characterization is to

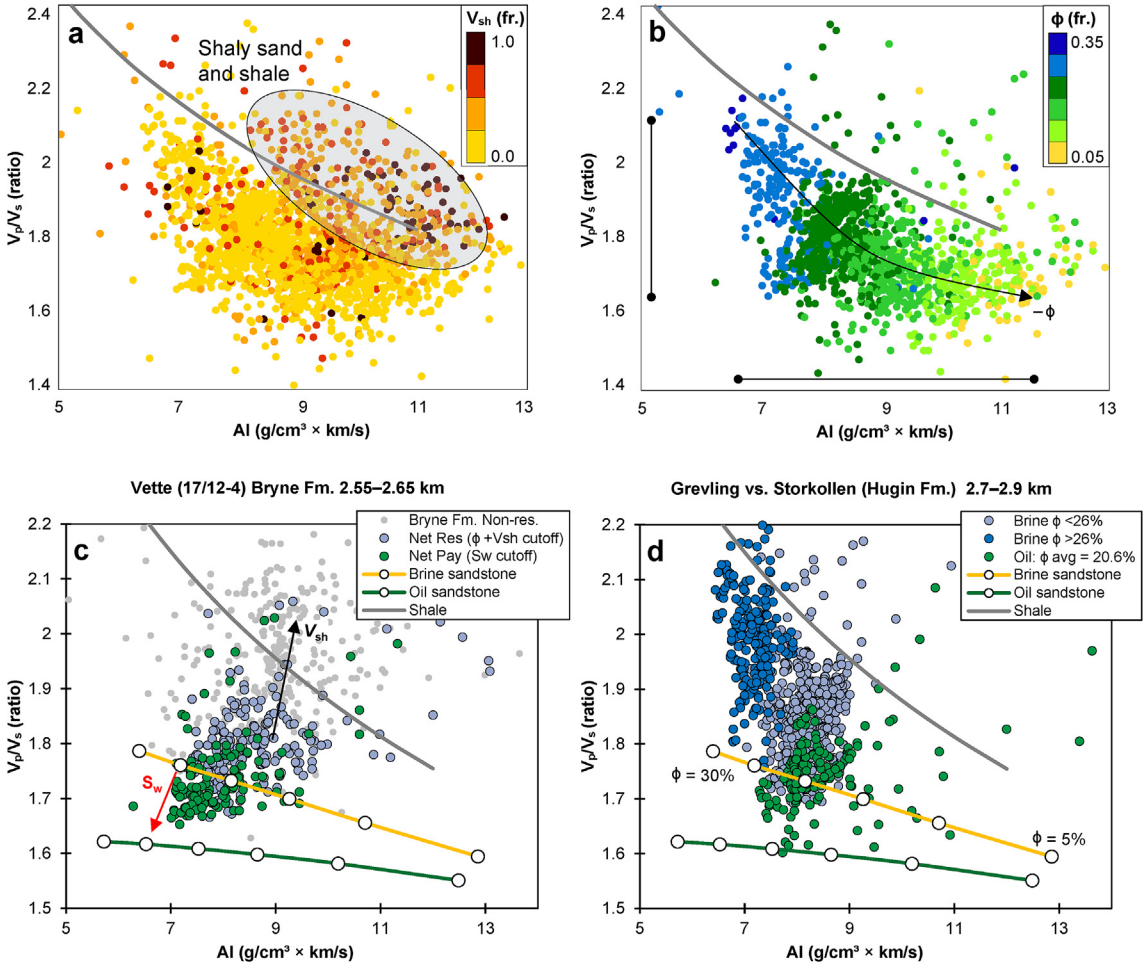

Fig. 9. V_P/V_S–AI crossplots highlighting the feasibility of analyzing reservoirs through seismic properties. Data from six wells (see Table 1) with shear velocity data is color coded with shale volume (a), and clean sand data only ($V_{sh} < 0.3$) is color coded with porosity (b). Reservoir sandstones at different depths indicate variable fluid discrimination, represented by the Vette discovery (c) and by comparing the Grevling discovery to the dry Storkollen prospect (d). (For interpretation of the references to color in this figure legend, the reader is referred to the Web version of this article.)

predict fluid content. Based on kerogen types and maximum potential burial of source rocks in the Egersund Basin and Ling Depression (Hansen et al., 2019), the expected hydrocarbon phase is oil, which has properties close to brine. Based on rock physics diagnostics, only the shallowest Jurassic reservoir data at 2.55–2.65 km BSF maximum burial indicate plausible ability to separate brine sand from hydrocarbon sand based on seismic properties (Fig. 9c). At this depth, we already expect the initial stages of quartz cement, which stiffens the grain framework and reduces fluid sensitivity. Data from oil- and brine-saturated Hugin Formation sandstones at 2.7–2.9 km burial depth largely overlap, indicating minor to negligible fluid separation in the V_P/V_S–AI attributes (Fig. 9d). There is a small decrease in average porosity from the brine sand compared to the slightly deeper oil-sand, yet we can infer that accounting for this difference would only further increase the degree of overlap based on the observed porosity trend (Fig. 9b). In combination, this suggests a required porosity of at least ~22–24% for enabling any meaningful separation based on the regional porosity–depth trend (Fig. 6e). For context, completely overlapping oil- and brine sand properties are found in Triassic sandstones at 3–3.2 km burial depth in the Grevling well, meaning that no fluid sensitivity is expected in elastic properties. A maximum burial depth of ~2.5–2.6 km mostly applies to the very shallowest structures in the studied region, meaning that exploration targeting Middle Jurassic reservoirs will face challenges related to fluid prediction.

AVO analysis can as an alternative, when carefully considering encasing shale properties and depth trends, aid fluid interpretation from seismic data (Avseth et al., 2008). Such analysis naturally complements the use of inverted elastic properties from seismic, but no prestack data were available for this study to further evaluate either of these approaches for our specific targets. From the conducted synthetic testing, changes in AVO attributes as a function of saturation are small compared to the inherent angle-dependent behavior of modeled sand-shale interfaces (Fig. 10). AVO class-changes corresponding to fluid substitution are observed in well 17/12-4, but this relationship will change rapidly with depth. Fig. 10b gives a good impression of the effect of reservoir porosity, represented by two sandstones in well 15/12-22 (Storkollen) with different porosities, and the lower-porosity Hugin Formation in the Grevling well. However, even when porosity is high, the fluid change has limited influence due to the small differences in petrophysical and elastic properties (i.e., density and bulk modulus) between oil and brine (Fig. 10b). The AVO class IV prediction is attributed to the large difference between cap rock and reservoir properties in the high-porosity Hugin sandstones in the Storkollen well. In this location, the Heather Formation is fairly hard (AI = 8–9 g/cm^3 × km/s), sandy to silty in the lower part and is fining upwards. On the other hand, the Egersund Formation in the Vette well is quite soft (AI = 6–7 g/cm^3 × km/s), resulting in the appearance of a hard, AVO class I Sandnes Formation sandstone underneath it. In both cases, our observations highlight that differences in cap rock properties have a far greater influence on the AVO behavior than the difference in fluid content for the studied wells. We inferred certain trends for the two different areas in terms of fluids and AVO classification, but the

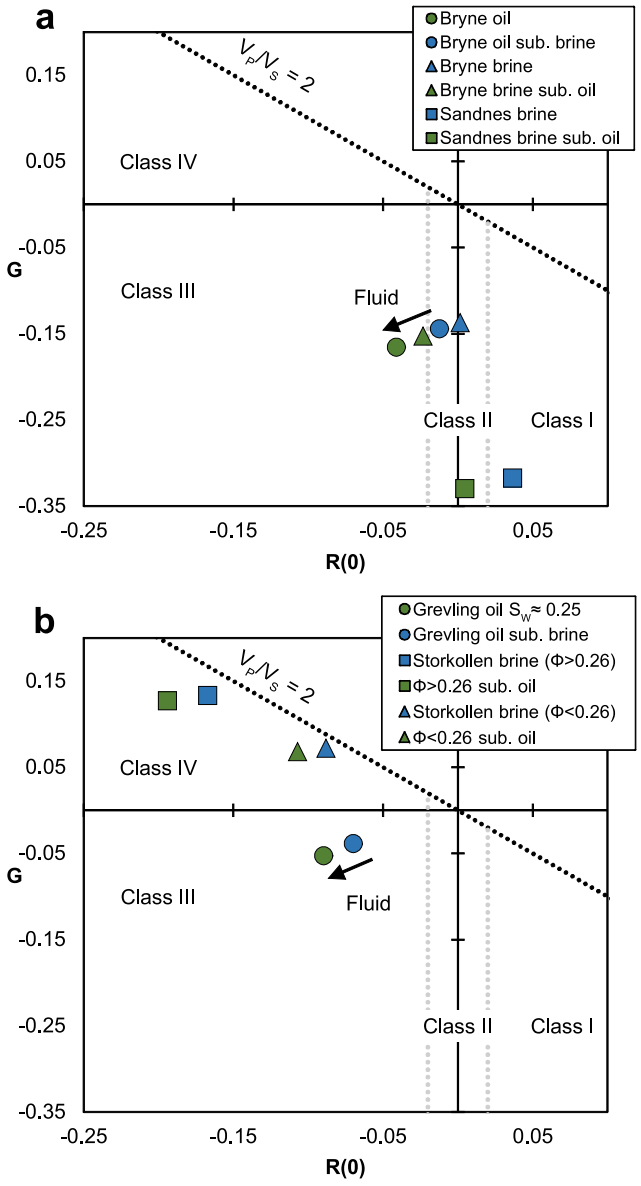

Fig. 10. Sensitivity test to fluid substitution on synthetic AVO signatures in the intercept–gradient crossplot. (a) Sandnes and Bryne formations in well 17/12-4 (Vette). (b) Hugin Formation in wells 15/12-21 (Grevling) and 15/12-22 (Storkollen).

maximum observed changes in R(0) and G between in-situ brine and in-situ oil in well 17/12-4 are −0.04 and −0.03, respectively, which are relatively discrete differences.

5.3. Relating reservoirs to source rocks and hydrocarbon kitchen

Considering previous discoveries, the thickness variations observed in seismic data, and local source rock burial (deep versus shallow), the Egersund Basin should have potential for hosting new discoveries. Particularly the great thicknesses observed in the Sandnes Formation, which is typically more consistent and clean in sandstone content compared to other formations, is favorable (Figs. 5 and 7). Depending on either fault juxtaposition of source and reservoir intervals (e.g., around well 9/2-1, Fig. 11) or pressure-induced expulsion stratigraphically downwards, the Sandnes Formation is also the most likely carrier bed for hydrocarbons. Conversely, the quality of the Bryne Formation is poorer close to the source rock, as evident in wells 9/2-1, 9/2-2 and 9/2-3. On the other hand, reservoir quality in the immediate proximity to the source rock is increasingly irrelevant the greater the volume of hydrocarbons that has been generated and expelled, which relates to possible migration distance. Older estimates based on basin modeling exist (e.g., Ritter, 1988; Hermanrud et al., 1990), but accurate quantification of actual generated hydrocarbon volumes and interpretation of possible migration pathways are sparse in public material. Importantly, these do not account for Cenozoic exhumation (Kalani et al., 2015a; Hansen et al., 2017; Baig et al., 2019), which would influence maximum burial depth and temperature in the models. Furthermore, microfracturing suggested to relate with the onset of kerogen cracking has been observed by Kalani et al. (2015b), indicating that minor maturation has occurred in some well locations.

Discoveries on the north flank of the basin (e.g., Vette and Mackerel) hint towards longer distance migration from the Egersund Basin kitchen, as no other source area is immediately apparent. Conversely, wells drilled on the south flank (e.g., well 9/4-5 which targeted Rotliegend Group sandstone) where good Sandnes Formation reservoirs are present close to the kitchen area, have so far been dry (Fig. 11). Lack of hydrocarbons in these wells could relate to migration issues across the large fault separating the kitchen and reservoir areas (Fig. 11). If the deeper parts of the Tau or Egersund formations in the Ling Depression (on the opposite side of Sele High) at some point generated significant amounts of hydrocarbons, there would likely have been more evidence of this in well 17/6-1 (Svaneøgle, minor oil shows) or 17/3-1 (Bark, small gas accumulation). In sum, oil in the Vette discovery is more likely to stem from the central Egersund Basin.

Lacking the ability to independently interpret fluid content from seismic amplitudes or inverted elastic properties instigate a greater focus on alternative and complementary methods of investigation. Such approaches could for instance involve more detailed modeling of the basin development, thermal history of source rocks (considering maximum burial and uplift episodes), and understanding of the most probable migration pathways (Iyer et al., 2018). Complementary, Hansen et al. (2019) investigated how relationships between elastic and geological properties in organic-rich shales could be incorporated in seismic source rock characterization. In any case, potential hydrocarbon accumulations can thus be predicted from a more geological perspective, and combined with information about changes and trends in reservoir quality and thickness. Altogether, this will help us better understand the nuances of the Jurassic petroleum system in the eastern Central North Sea region.

6. Conclusions

For further exploration of the eastern Central North Sea, a region with many dry wells, it is important to consider and understand all parts of the petroleum system. There are clearly issues related to overall source rock maturation, but successful wells in certain areas prove local oil generation. In that context, we focus on reservoir quality variations, thickness differences and potential target formations in areas where hydrocarbon generation and migration can plausibly occur. The main outcomes of this analysis are as follows:

- The Sandnes Formation is a good reservoir target in the central Egersund Basin and on the south flank (gross thickness 80–147 m, N/G = 33–93%), but generally poorer thickness (16–26 m) and variable quality (N/G = 11–81%) are found farther northwest (i.e., Egersund Basin north flank and Ling Depression).
- The Bryne Formation has poorer reservoir quality due to porosity deterioration and heterogeneity in the central Egersund Basin (N/G < 20%), but good sandstones are found at shallower depths on the flanks and partially in the Ling Depression (N/G = 25–70%).
- The Hugin Formation generally exhibits excellent quality, but rapid thickness differences (28–154 m) and local development are observed in the study area.
- Intermediate thickness (28–63 m) and reservoir quality (N/

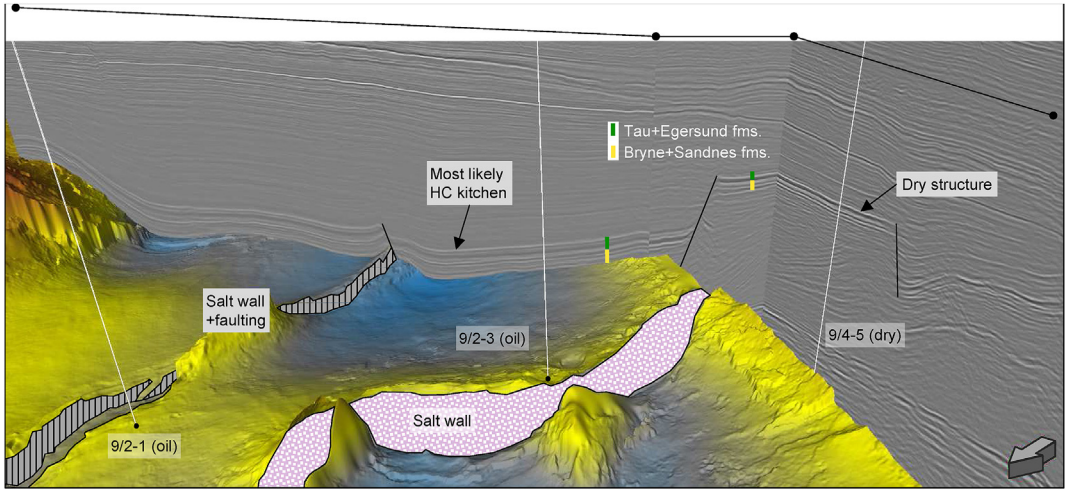

Fig. 11. The 4-way closure structure across the large fault near the deepest source rock burial in the Egersund Basin was found dry (well 9/4-5, close to 2D line). The draped base Bryne horizon time-structure grid illustrates the general basin configuration. The 3D arbitrary line on the left side of the image has opposite polarity in comparison to the two 2D composite sections covering the structure.

G = 27–43%) are recognized in the Sleipner Formation based on our limited sample pool. Thicknesses surpassing that observed in wells, apparently related to salt structures and faults, are clear on seismic reflection data. Subtle depositional features on the seismic scale have also been identified, which could be an indicator of thicker fluvial channel sandstones to target compared with the Bryne Formation.

Rock physics diagnostics of well-log data demonstrate the feasibility of predicting lithology, porosity and fluids from different types of seismic data. In this context, we further discuss connections and challenges with source rock intervals and potential migration. The observed fluid sensitivity in the case of oil at relevant reservoir depths indicates that more geologically driven approaches could be advantageous to explore for predicting potential hydrocarbon accumulations in the study area.

Acknowledgements

The authors are grateful to Vår Energi AS (previously Eni Norge) for funding and supporting the “ReSource – Quantitative analysis of reservoir, cap, and source rocks of the Central North Sea” R&D project. This work was carried out at the University of Oslo with academic licenses for Petrel (Schlumberger), Interactive Petrophysics (Lloyd's Register) and Hampson-Russell (CGG) commercial software packages. All data are courtesy of the Norwegian Petroleum Directorate (NPD) through the DISKOS national data repository.

Appendix A. Supplementary data

Supplementary data to this article can be found online at https://doi.org/10.1016/j.marpetgeo.2019.08.044.

References

Asquith, G., Krygowski, D.A., 2004. Basic Well Log Analysis, second ed. AAPG, Tulsa.
Avseth, P., Dræge, A., van Wijngaarden, A.-J., Johansen, T.A., Jørstad, A., 2008. Shale rock physics and implications for AVO analysis: a North Sea demonstration. Lead. Edge 27, 788–797. https://doi.org/10.1190/1.2944164.
Baig, I., Faleide, J.I., Mondol, N.H., Jahren, J., 2019. Burial and exhumation history controls on shale compaction and thermal maturity along the Norwegian North Sea basin margin areas. Mar. Pet. Geol. 104, 61–85. https://doi.org/10.1016/j.marpetgeo.2019.03.010.
Bjørlykke, K., 1998. Clay mineral diagenesis in sedimentary basins — a key to the prediction of rock properties. Examples from the North Sea Basin. Clay Miner. 33, 15–34.
Bjørlykke, K., Ramm, M., Saigal, G.C., 1989. Sandstone diagenesis and porosity modification during basin evolution. Geol. Rundsch. 78, 243–268.
Doré, A.G., Jensen, L.N., 1996. The impact of late Cenozoic uplift and erosion on hydrocarbon exploration: offshore Norway and some other uplifted basins. Glob. Planet. Chang. 12, 415–436. https://doi.org/10.1016/0921-8181(95)00031-3.
Faleide, J.I., Tsikalas, F., Breivik, A.J., Mjelde, R., Ritzmann, O., Engen, Ø., Wilson, J., Eldholm, O., 2008. Structure and evolution of the continental margin off Norway and the Barents Sea. Episodes 31, 82–91.
Faleide, J.I., Bjørlykke, K., Gabrielsen, R.H., 2015. Geology of the Norwegian continental shelf. In: Bjørlykke, K. (Ed.), Petroleum Geoscience. From Sedimentary Environments to Rock Physics, second ed. Springer-Verlag Berlin Heidelberg, pp. 603–638. https://doi.org/10.1007/978-3-642-34132-8.
Folkestad, A., Satur, N., 2008. Regressive and transgressive cycles in a rift-basin: depositional model and sedimentary partitioning of the Middle Jurassic Hugin formation, southern Viking graben, North Sea. Sediment. Geol. 207, 1–21. https://doi.org/10.1016/j.sedgeo.2008.03.006.
Halland, E.K., Gjeldvik, I.T., Johansen, W.T., Magnus, C., Meling, I.M., Pedersen, S., Riis, F., Solbakk, T., Tappel, I., 2011. CO2 Storage Atlas - Norwegian North Sea. Norwegian Petroleum Directorate, Stavanger, Norway.
Hansen, J.A., Yenwongfai, H.D., Fawad, M., Mondol, N.H., 2017. Estimating exhumation using experimental compaction trends and rock physics relations, with continuation into analysis of source and reservoir rocks: central North Sea, offshore Norway. In: 88th Annual International Meeting, Expanded Abstracts, pp. 3971–3975. https://doi.org/10.1190/segam2017-17783053.1.
Hansen, J.A., Mondol, N.H., Fawad, M., 2019. Organic content and maturation effects on elastic properties of source rock shales in the Central North Sea. Interpretation 7, T477–T497. https://doi.org/10.1190/INT-2018-0105.1.
Hermanrud, C., Eggen, S., Jacobsen, T., Carlsen, E.M., Pallesen, S., 1990. On the accuracy of modelling hydrocarbon generation and migration: the Egersund Basin oil find, Norway. Org. Geochem. 16, 389–399. https://doi.org/10.1016/0146-6380(90)90056-6.
Iyer, K., Schmid, D.W., Rüpke, L.H., Skeie, J.E., 2018. Importance of evolving fault seals on petroleum systems: southern Halten terrace, Norwegian Sea. AAPG (Am. Assoc. Pet. Geol.) Bull. 102, 671–689. https://doi.org/10.1306/0208171616417017.
Jackson, C.A.-L., Chua, S.-T., Bell, R.E., Magee, C., 2013. Structural style and early stage growth of inversion structures: 3D seismic insights from the Egersund Basin, offshore Norway. J. Struct. Geol. 46, 167–185. https://doi.org/10.1016/j.jsg.2012.09.005.
Jordt, H., Faleide, J.I., Bjørlykke, K., Ibrahim, M.T., 1995. Cenozoic sequence stratigraphy of the central and northern North Sea Basin: tectonic development, sediment distribution and provenance areas. Mar. Pet. Geol. 12, 845–879. https://doi.org/10.1016/0264-8172(95)98852-V.
Kalani, M., Jahren, J., Mondol, N.H., Faleide, J.I., 2015a. Compaction processes and rock properties in uplifted clay dominated units - the Egersund Basin, Norwegian North Sea. Mar. Pet. Geol. 68, 596–613. https://doi.org/10.1016/j.marpetgeo.2014.08.015.
Kalani, M., Jahren, J., Mondol, N.H., Faleide, J.I., 2015b. Petrophysical implications of source rock microfracturing. Int. J. Coal Geol. 143, 43–67. https://doi.org/10.1016/j.coal.2015.03.009.
Kieft, R.L., Jackson, C.A.-L., Hampson, G.J., Larsen, E., 2010. Sedimentology and sequence stratigraphy of the Hugin formation, quadrant 15, Norwegian sector, South Viking graben. In: Vining, B.A., Pickering, S.C. (Eds.), Petroleum Geology: from Mature Basins to New Frontiers – Proceedings of the 7th Petroleum Geology Conference. Geological Society, London, pp. 157–176. https://doi.org/10.1144/0070157.
Larionov, V., 1969. Radiometry of Boreholes (In Russian). Nedra, Moscow.
Maast, T.E., Jahren, J., Bjørlykke, K., 2011. Diagenetic controls on reservoir quality in Middle to upper Jurassic sandstones in the south Viking graben, North Sea. AAPG (Am. Assoc. Pet. Geol.) Bull. 95, 1937–1958. https://doi.org/10.1306/03071110122.

Mannie, A.S., Jackson, C.A.-L., Hampson, G.J., 2014. Structural controls on the stratigraphic architecture of net-transgressive shallow-marine strata in a salt-influenced rift basin: Middle-to-Upper Jurassic Egersund Basin, Norwegian North Sea. Basin Res. 26, 675–700. https://doi.org/10.1111/bre.12058.

Mannie, A.S., Jackson, C.A.-L., Hampson, G.J., Fraser, A.J., 2016. Tectonic controls on the spatial distribution and stratigraphic architecture of a net-transgressive shallow-marine synrift succession in a salt-influenced rift basin: Middle to Upper Jurassic, Norwegian Central North Sea. J. Geol. Soc. 173, 901–915. https://doi.org/10.1144/jgs2016-033.

Marcussen, Ø., Maast, T.E., Mondol, N.H., Jahren, J., Bjørlykke, K., 2010. Changes in physical properties of a reservoir sandstone as a function of burial depth – the Etive Formation, northern North Sea. Mar. Pet. Geol. 27, 1725–1735. https://doi.org/10.1306/08220808044.

Mondol, N.H., Bjørlykke, K., Jahren, J., 2008. Experimental compaction of clays: relationship between permeability and petrophysical properties in mudstones. Pet. Geosci. 14, 319–337. https://doi.org/10.1144/1354-079308-773.

Morad, S., Al-Ramadan, K., Ketzer, J.M., De Ros, L.F., 2010. The impact of diagenesis on the heterogeneity of sandstone reservoirs: a review of the role of depositional facies and sequence stratigraphy. AAPG (Am. Assoc. Pet. Geol.) Bull. 94, 1267–1309.

NPD, 2019. Norwegian Petroleum Directorate Fact Pages. http://factpages.npd.no/factpages/.

Ødegaard, E., Avseth, P., 2004. Well log and seismic data analysis using rock physics templates. First Break 23, 37–43. https://doi.org/10.3997/1365-2397.2004017.

Peltonen, C., Marcussen, Ø., Bjørlykke, K., Jahren, J., 2009. Clay mineral diagenesis and quartz cementation in mudstones: the effects of smectite to illite reaction on rock properties. Mar. Pet. Geol. 26, 887–898.

Ritter, U., 1988. Modelling of hydrocarbon generation patterns in the Egersund sub-basin, North Sea. Adv. Org. Geochem. 13, 165–174. https://doi.org/10.1016/0146-6380(88)90036-8.

Shuey, R.T., 1985. A simplification of the Zoeppritz equations. Geophysics 50, 609–614. https://doi.org/10.1190/1.1441936.

Vollset, J., Doré, A.G., 1984. A Revised Triassic and Jurassic Lithostratigraphic Nomenclature for the Norwegian North Sea. NPD-Bulletin, 3. Norwegian Petroleum Directorate, pp. 53.

Ziegler, P.A., 1992. North Sea rift system. Tectonophysics 208, 55–75. https://doi.org/10.1016/0040-1951(92)90336-5.